Available online at www.sciencedirect.com

SciVerse ScienceDirect

Ceramics International 39 (2013) 3337–3344

CERAMICS INTERNATIONAL

www.elsevier.com/locate/ceramint

Thermal decomposition approach for the synthesis of silver–alumina nanocomposite powders

Ravi Kant Sharma, P. Jeevanandam*

Department of Chemistry, Indian Institute of Technology Roorkee, Roorkee 247667, India

Received 12 August 2012; received in revised form 21 September 2012; accepted 5 October 2012
Available online 12 October 2012

Abstract

Silver–alumina nanocomposite powders have been synthesized by a simple thermal decomposition approach using silver acetate and alumina. The effect of using nanocrystalline versus macro-crystalline alumina during the preparation of the nanocomposites has been investigated. The nanocomposites were characterized by powder X-ray diffraction, Fourier transform infrared spectroscopy, thermal gravimetric analysis, surface area measurements, field emission scanning electron microscopy coupled with energy dispersive X-ray analysis, transmission electron microscopy and diffuse reflectance spectroscopy. The characterization results indicate the presence of silver nanoparticles on the surface of alumina and nanocrystalline alumina acts as a better support for the dispersion of silver nanoparticles compared to the macro-crystalline alumina. The silver–alumina nanocomposite powders have been explored as catalysts for the reduction of 4-nitrophenol.

Keywords: Silver based nanocomposite powders; Alumina; Thermal decomposition; Catalytic reduction

1. Introduction

Silver based nanocomposites exhibit interesting optical properties and antimicrobial activity while alumina is widely used in different fields because of its interesting characteristics such as easy availability, low cost, low toxicity, ease of synthesis, good optical transparency, high refractive index, high melting point, hydrophobicity, mechanical strength, dielectric behavior, electrical insulating property and thermal and chemical stability [1–4]. Fine alumina powders and their compacts are commonly used as adsorbents, catalysts and catalytic supports due to their high surface area [5,6]. Alumina behaves as a Lewis acid and is used as an absorbent for the removal of toxic metal oxyanions from water (e.g. arsenate) [7].

Silver–alumina nanocomposite powders are interesting due to their applications in antimicrobial activity, $DeNO_x$ activity, catalysis, optics, micro-electronics, imaging and sensors [8–14]. Recently, many authors have reported that silver nanoparticles impregnated on different supports can be used as catalysts for the reduction of aromatic nitro-compounds [15–19]. The acidic nature of alumina is reported to be the main factor to stabilize the active state of the metal species [20].

Silver–alumina nanocomposite powders have been synthesized by different methods such as the solvothermal [10], micro-emulsion [14], co-precipitation [20], pulsed laser deposition [21], gel casting [22], sol–gel [23] and sonochemical method [24]. These methods usually take long time for the synthesis or require sophisticated apparatus. In the present study, the synthesis of silver–alumina nanocomposite powders by a simple quick thermal decomposition method has been reported. The effect of using nanocrystalline versus macro-crystalline alumina has also been investigated. After characterization, the nanocomposites have been explored as catalysts for the reduction of 4-nitrophenol to 4-aminophenol using $NaBH_4$.

2. Experimental

The chemicals used were aluminum isopropoxide, toluene, ammonia solution (25%), silver acetate, diphenyl ether,

*Corresponding author. Tel.: +91 1332 285444; fax: +91 1332 286202.
E-mail address: jeevafcy@iitr.ernet.in (P. Jeevanandam).

0272-8842/$ - see front matter © 2012 Elsevier Ltd and Techna Group S.r.l. All rights reserved.
http://dx.doi.org/10.1016/j.ceramint.2012.10.023

methanol, commercial alumina (macro-crystalline alumina), 4-nitrophenol and $NaBH_4$ and were used as received. First, alumina nanoparticles were prepared followed by the synthesis of nanocomposites and more details on the synthesis are as follows.

Alumina nanoparticles were prepared using minor modification of the sol–gel method [25]. About 1.86 g of aluminum isopropoxide, 40 mL of ethanol, 25 mL of toluene and 0.5 mL of water (Millipore®) were taken in a 100 mL round bottom flask. The contents were vigorously stirred for 3 h at room temperature till the mixture became milky white. Then, 2 mL of 25% ammonia solution was added followed by the addition of about 1 mL of water after 1 h. The contents were kept for constant stirring for about 24 h at room temperature. The obtained slurry was evaporated at 80 °C to form a gel and it was dried at 80 °C overnight to obtain a white powder. The powder was calcined in air at 500 °C for 3 h inside a muffle furnace (Nabertherm®) to obtain the alumina nanoparticles.

Silver–alumina nanocomposite powders were prepared by the thermal decomposition of silver acetate in diphenyl ether in the presence of alumina (nanocrystalline alumina/macro-crystalline alumina). The effect of using alumina with or without activation was also investigated. Different silver–alumina nanocomposite powders were synthesized by varying concentration of the silver acetate (0.25–1 mmol) and the synthesis details along with nomenclature of the synthesized nanocomposite powders are given in Table 1. More details on the synthesis procedure are as follows. About 0.04 g (0.25 mmol), 0.08 g (0.5 mmol), or 0.16 g (1 mmol) of silver acetate and 0.10 g (1 mmol) of alumina (nanocrystalline or macro-crystalline) were added to 10 mL diphenyl ether in a 50 mL round bottom flask. The contents were refluxed at 200 °C/225 °C for about 30 min (in the case of macro-crystalline alumina, the contents were refluxed at 225 °C due to incomplete decomposition of silver acetate at 200 °C, as observed by the XRD results). The slurries obtained were cooled to room temperature. Then, about 30 mL of methanol was added and the contents were centrifuged for about 20 min. The precipitates were washed with methanol and dried at ~80 °C overnight. The powders were calcined in air at 350 °C for 3 h inside the muffle furnace to remove the solvent and organic impurities present in the nanocomposite powders. The color of the silver–alumina nanocomposite powders was gray.

Powder XRD patterns were recorded using a Brucker AXS D8 diffractometer operating with Cu-Kα radiation ($\lambda = 1.5406$ Å) with a scanning speed of 2°/min. A Thermo Nicolet Nexus FT-IR spectrophotometer was used for recording IR spectra of the nanocomposite powders using KBr pellets. Thermo gravimetric measurements were carried out in the temperature range 25–1000 °C using a Perkin Elmer (Pyris Diamond) instrument in N_2 atmosphere at a heating rate of 5°/min. The specific surface area of the nanocomposite powders was measured using the Brunauer–Emmett–Teller (BET) method by a Micromeritics Chemisorb 2720 instrument using N_2 physisorption. Morphologies of the samples along with elemental analysis (EDXA) data were obtained using a FEI Quanta 200F microscope operating at 20 kV. TEM images of the nanocomposite powders were recorded using a FEI TECNAI G2 electron microscope operating at an accelerating voltage of 200 kV. Diffuse reflectance spectra were recorded using a Shimadzu UV-2450 UV–visible spectrophotometer attached with a diffuse reflectance accessory in the wavelength range 200–800 nm using $BaSO_4$ as the reference.

The catalytic activity of the silver–alumina nanocomposite powders was tested using the reduction of 4-nitrophenol to 4-aminophenol using $NaBH_4$ as the reducing agent [14]. This reaction has been used to test the catalytic activity of different nanostructured materials [17,18]. To about 50 mL aqueous solution of 4-nitrophenol (0.1 mmol), 50 mL of freshly prepared aqueous solution of $NaBH_4$ (0.53 M) was added. Then, about 20 mg of the catalyst (silver–alumina nanocomposite powders) was added and the contents were kept for constant stirring at room temperature. Complete reduction of 4-nitrophenol (yellow colored solution) to 4-aminophenol was indicated by decolorization of the solution and the time taken for the same was noted.

Table 1
Synthesis details and nomenclature of the silver–alumina nanocomposite powders.

Sl. no.	Sample ID	Amount of silver acetate used (mmol)	Al_2O_3 type used	Color of the nanocomposite powder	Yield (g)
1	S-1	1	Sol–gel alumina with calcination	Gray	0.18
2	S-2	1	Sol–gel alumina without calcination	Gray	0.33
3	S-3	0.5	Sol–gel alumina with calcination	Gray	0.12
4	S-4	0.5	Sol–gel alumina without calcination	Gray	0.12
5	S-5	0.25	Sol–gel alumina with calcination	Gray	0.10
6	S-6	0.25	Sol–gel alumina without calcination	Gray	0.10
7	S-7	1	Commercial alumina with calcination	Gray	0.19
8	S-8	1	Commercial alumina without calcination	Gray	0.13
9	S-9	0.5	Commercial alumina with calcination	Gray	0.14
10	S-10	0.5	Commercial alumina without calcination	Gray	0.13
11	S-11	0.25	Commercial alumina with calcination	Gray	0.11
12	S-12	0.25	Commercial alumina without calcination	Gray	0.11

3. Results and discussion

Powder XRD pattern of the nanocrystalline (sol–gel) alumina before calcination showed peaks due to boehmite (JCPDS file no. 01-0774). After calcination at 500 °C, peaks due to γ-Al_2O_3 (JCPDS file no. 29-0063) were observed. The XRD patterns of the silver–nanocrystalline alumina nanocomposite powders before calcination showed peaks only due to silver (JCPDS file no. 03-0921). After calcination at 350 °C, the nanocomposite powders (Fig. 1a) show weak reflections at $2\theta \approx 19.3^\circ$ and 33.8° due to $AgAlO_2$ (JCPDS file no. 21-1070). The XRD patterns of silver–macro-crystalline alumina nanocomposite powders before and after calcination (Fig. 1b) show peaks due to silver (JCPDS file no. 03-0921) and a small peak due to γ-Al_2O_3 (JCPDS file no. 29-0063).

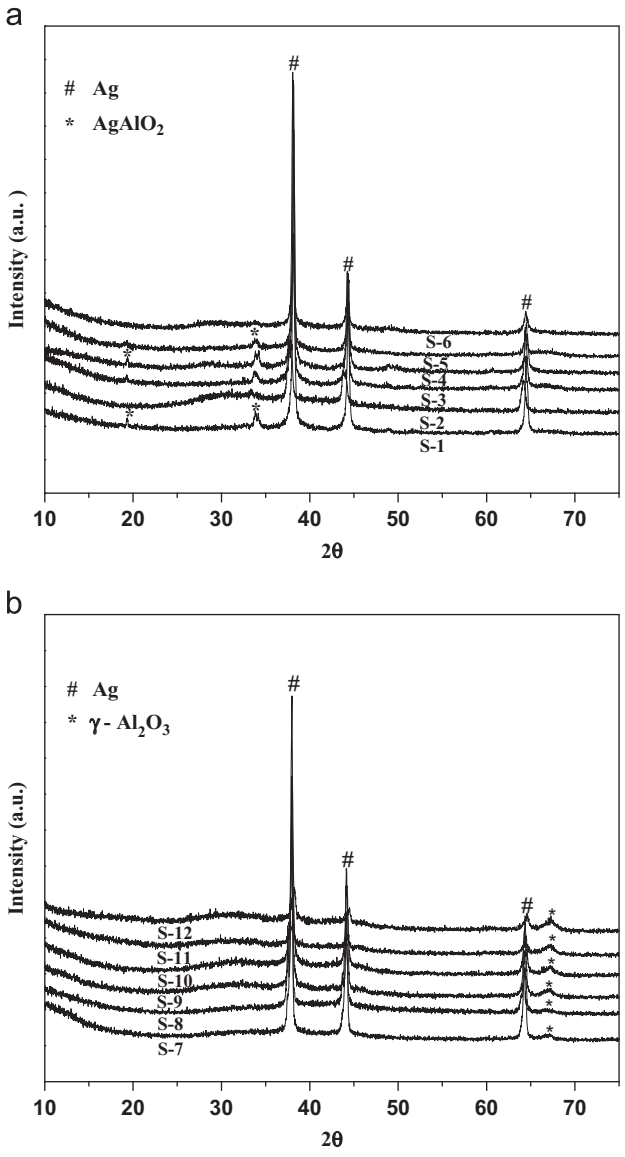

Fig. 1. XRD patterns of (a) silver–nanocrystalline alumina nanocomposite powders after calcination, and (b) silver–macro-crystalline alumina nanocomposite powders after calcination. The synthesis details of the nanocomposite powders are given in Table 1.

The crystallite size for pure nanocrystalline alumina and the silver nanoparticles present in the silver–alumina nanocomposite powders (after calcination at 350 °C) was calculated using the Debye–Scherrer formula [26]. The crystallite size of nanocrystalline alumina before and after calcination was 3 nm and 3.2 nm, respectively. The crystallite size of silver nanoparticles varied from 13.0 to 38.9 nm in the nanocomposite powders prepared using nanocrystalline alumina and in the case of silver–macro-crystalline alumina nanocomposite powders, the size varied from 15.5 to 39.9 nm.

Thermal gravimetric analysis of pure nanocrystalline alumina (as prepared) showed more weight loss (34.7%) compared to macro-crystalline alumina (7.3%). The silver–nanocrystalline alumina nanocomposite powders also showed more overall weight loss (8.6–24.0%) up to about 500 °C compared to the silver–macro-crystalline alumina nanocomposite powders (3.2–9.6%). The weight loss below 150 °C is attributed to the removal of physisorbed water molecules. The weight loss in the region 150–500 °C is attributed to the dehydration of AlOOH to Al_2O_3 and also the removal of organic impurities.

IR spectral measurements were carried out for pure alumina as well as for the silver–alumina nanocomposite powders. Bands near 3500 cm^{-1} due to O–H stretching were observed and weak bands at about 2930 and 2858 cm^{-1} were attributed to C–H stretching [5]. The bands at about 1644 cm^{-1} were attributed to the bending vibration of water molecules [6]. The bands observed between 1585 and 1387 cm^{-1} in the nanocomposite powders before calcination were attributed to the presence of (C=O), carbon–carbon (C–C) and carbon–hydrogen (C–H) vibrations [5,25] and these bands almost disappeared after calcination. The bands at about 1168 cm^{-1} and 1070 cm^{-1} in the case of nanocomposite powders before calcination were attributed to ν_{asym}.Al–O–H and ν_{sym}.Al–O–H vibrations of boehmite, respectively [5]. These bands also disappeared after calcination. The band near 884 cm^{-1} was attributed to the Al–O bond [27] and the bands near 639 and 480 cm^{-1} in all the nanocomposite powders (S-1–S-6) were attributed to the bending modes of AlO_6 units while the bands near 752 and 783 cm^{-1} were attributed to the bending vibration of AlO_4 group [25]. The IR spectra of silver–macro-crystalline alumina nanocomposite powders before and after calcination (nanocomposites S-7–S-12) showed similar IR features as observed in the case of silver–nanocrystalline alumina nanocomposite powders.

Surface area measurements (BET) were carried out for nanocrystalline alumina, macro-crystalline alumina, and silver–alumina nanocomposite powders (S-6 and S-12). Nanocrystalline alumina had high specific surface area (525.7 $m^2\,g^{-1}$) and total pore volume (0.26 $cm^3\,g^{-1}$) compared to that of macro-crystalline alumina (surface area $\sim$101.9 $m^2\,g^{-1}$ and total pore volume $\sim$0.05 $cm^3\,g^{-1}$). The silver–nanocrystalline alumina nanocomposite powder (S-6) had high specific surface area (267.4 $m^2\,g^{-1}$) and

total pore volume ($0.13\ cm^3\ g^{-1}$) compared to those of silver–macro-crystalline alumina nanocomposite powder (S-12) (surface area: $60.3\ m^2\ g^{-1}$ and total pore volume: $0.03\ cm^3\ g^{-1}$).

The EDX analysis results indicated the presence of carbon, oxygen, aluminum and silver in the nanocomposite powders. The weight percent of Ag varied from about 4.4% to 48.4% in the silver–nanocrystalline alumina nanocomposite powders (S-1–S-6) and it varied from about 16.5% to 84.0% in silver–macro-crystalline alumina nanocomposite powders (S-7–S-12). When nanocrystalline alumina (with or without calcination) and macro-crystalline alumina (after calcination) were employed (nanocomposite powders, S-1–S-6 and S-7, S-9, S-11), with increase in concentration of the silver acetate (0.25–1 mmol), the silver weight percent also increased (about 5–61.3%) in the nanocomposite powders. On the other hand, the weight percent of silver remained the same (about 50%) in the case of nanocomposite powders prepared using macro-crystalline alumina without calcination (S-8, S-10, and S-12). The EDXA data indicated uniform distribution of Ag in the silver–nanocrystalline alumina nanocomposite powders compared to silver–macro-crystalline alumina nanocomposite powders.

Typical TEM images for the nanocrystalline alumina, silver–nanocrystalline alumina nanocomposite powders (S-1, S-2 and S-6) and silver–macro-crystalline alumina nanocomposite powders (S-7, S-8 and S-12) are shown in Figs. 2 and 3, respectively. The average particle size for nanocrystalline and macro-crystalline alumina was estimated to be 11.5 ± 2.5 nm and 98.5 ± 19.5 nm, respectively. The TEM images indicate that the silver nanoparticles are finely dispersed on nanocrystalline alumina compared to that on macro-crystalline alumina. The average particle size of the silver nanoparticles was estimated for the nanocomposite powders S-1, S-2 and S-6 (in which the silver nanoparticles are not agglomerated) and the values are 8.2 ± 2.1 nm, 23.6 ± 0.2 nm and 8.9 ± 1.4 nm, respectively.

The TEM results reported in the literature for the silver–alumina nanocomposite powders synthesized by different methods such as gel casting [22], wet chemical [4], and sol–gel methods [28,29] show non-uniform distribution of silver nanoparticles on alumina. A few methods such as sonochemical [24] and solvothermal synthesis [10] lead to

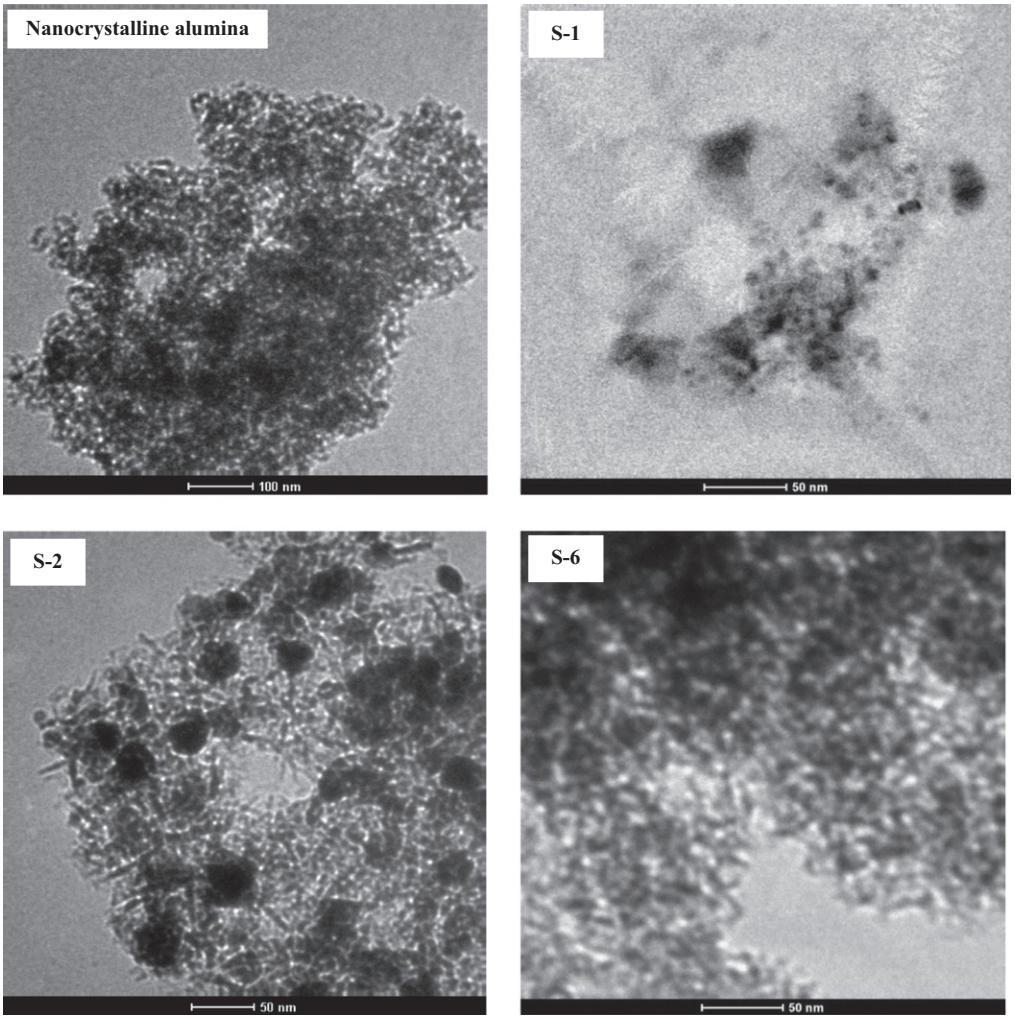

Fig. 2. TEM images of nanocrystalline alumina and silver–nanocrystalline alumina nanocomposite powders.

uniform distribution of silver nanoparticles on alumina but the sonochemical method requires continuous flow of $Ar–H_2$ mixture throughout the reaction. In the case of solvothermal method, the calcination temperature is high (e.g. 550 °C), whereas in the present study, the required calcination temperature is only 350 °C. The proposed thermal decomposition method is simple and leads to fairly uniform distribution of silver nanoparticles on alumina at a relatively lower calcination temperature.

Diffuse reflectance spectra of silver–nanocrystalline alumina nanocomposite powders are shown in Fig. 4a. The nanocomposite powders show surface plasmon resonance band at about 430 nm due to the presence of nanocrystalline silver. The silver–macro-crystalline alumina nanocomposite powders do not show the characteristic SPR band of nanocrystalline silver (Fig. 4b). This is attributed to non-uniform distribution of bigger silver nanoparticles on macro-crystalline alumina (as confirmed by the EDXA results).

$Ag–Al_2O_3$ nanocomposite powders have been synthesized by various authors. For example, Bala et al. [4] have synthesized the nanocomposite using the wet chemical method and Haji et al. [22] have reported the synthesis by gel casting. Both the methods require longer reaction times (15 h and 24 h, respectively). In addition, the wet chemical method needs a reducing agent (e.g. sodium borohydride) and the gel casting synthesis requires a dispersant (e.g. Dolapix ET85). The synthesis of silver–alumina nanocomposite powders by the thermal decomposition method is simple and quick (30 min) and the method does not require any additional reagent. The present synthesis method also leads to nanocomposite powders with higher surface area compared to the literature methods. For example, the specific surface areas of $Ag–Al_2O_3$ nanocomposite powders synthesized by the solvothermal method [10] and the sonochemical method [24] are about 141 m^2/g and 232 m^2/g, respectively. The $Ag–Al_2O_3$ nanocomposite powder prepared by the present thermal decomposition method possesses a higher surface area (267.4 m^2/g). Moreover, the effect of using nanocrystalline versus macro-crystalline alumina on the characteristics of final nanocomposite powders has been investigated for the first time in the present study.

The catalytic activity of the silver–alumina nanocomposite powders was tested using the reduction of 4-nitrophenol (4-NP) to 4-aminophenol (4-AP) by sodium borohydride.

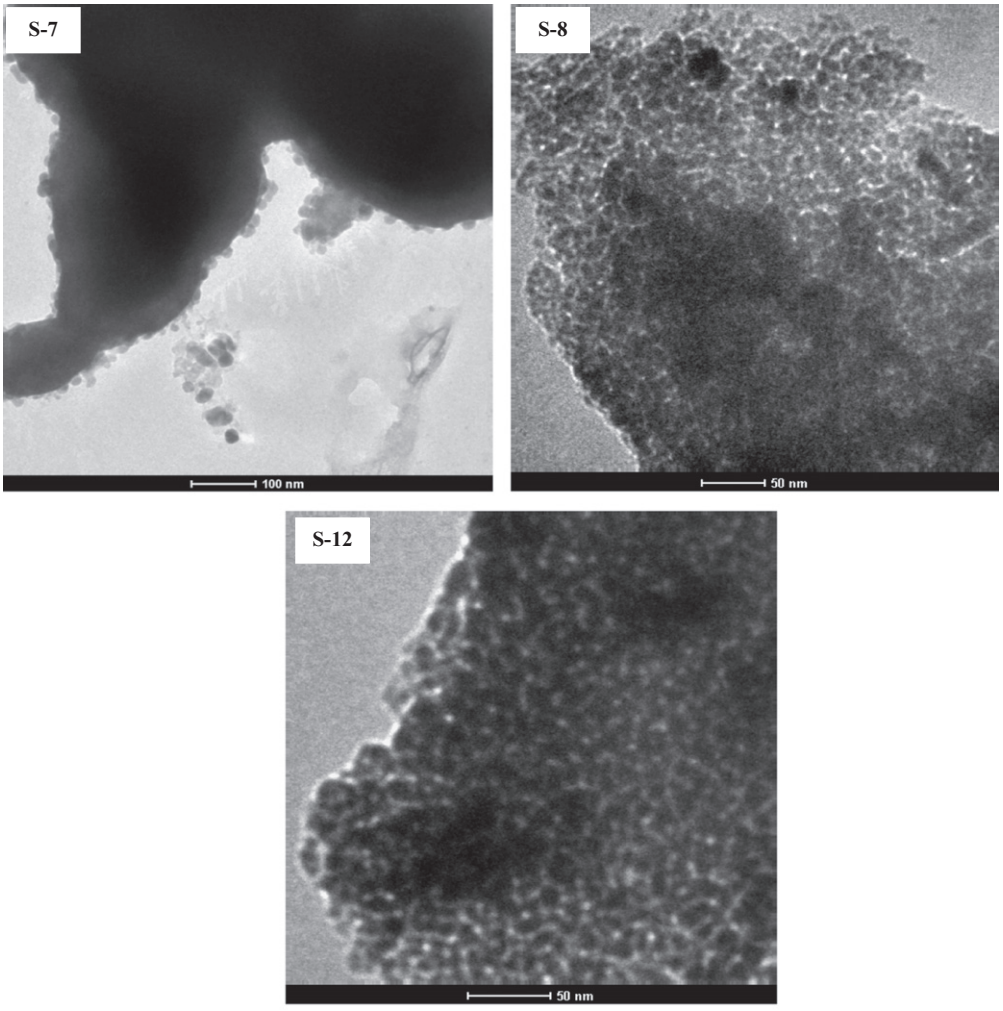

Fig. 3. TEM images of silver–macro-crystalline alumina nanocomposite powders.

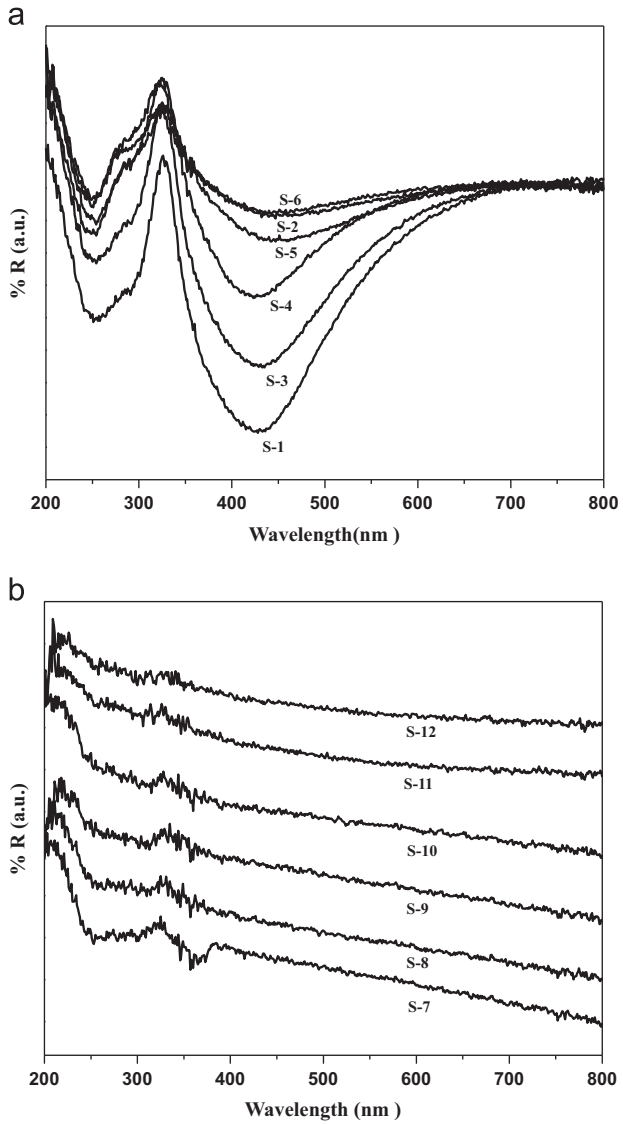

Fig. 4. Diffuse reflectance spectra of (a) silver–nanocrystalline alumina nanocomposite powders and (b) silver–macro-crystalline alumina nanocomposite powders.

The reduction of 4-nitrophenol with $NaBH_4$ was also carried out in the absence of the catalyst. The time required for the complete reduction of 4-nitrophenol, as indicated by the decolorization when different nanocomposite powders were used as catalysts, is given in Table 2. It can be noticed that the reduction of 4-nitrophenol does not take place in the absence of the catalyst. Also, the reduction of 4-nitrophenol does not occur when pure nanocrystalline alumina or macro-crystalline alumina is used as the catalyst. The silver–nanocrystalline alumina nanocomposite powders (time of reduction: 4–20 s) and the silver–macro-crystalline alumina nanocomposite powders (time of reduction: 240–1020 s) act as better catalysts compared to pure Ag nanoparticles (time of reduction: 1320 s). The performance of silver–nanocrystalline alumina nanocomposite powders (S1–S6) is better compared to that of silver–macro-crystalline alumina nanocomposite powders (S7–S12). Silver nanoparticles are highly dispersed on the surface of

Table 2
Time required for the complete reduction of 4-nitrophenol in the presence of silver–alumina nanocomposite powders as catalysts.

Catalyst	Time required for the reduction (s)
No catalyst	No reduction
Pure Ag nanoparticles	1320
Pure sol–gel alumina	No reduction
Pure commercial alumina	No reduction
S-1	15
S-2	6
S-3	20
S-4	5
S-5	6
S-6	4
S-7	240
S-8	480
S-9	480
S-10	240
S-11	1020
S-12	540

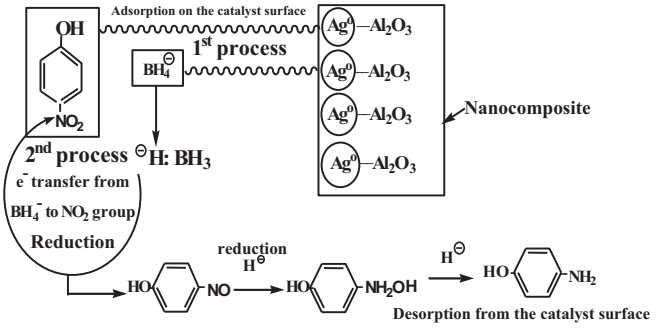

Fig. 5. Schematic indicating the mechanism of reduction of 4-nitrophenol to 4-aminophenol in the presence of silver–alumina nanocomposite powders as catalysts.

nanocrystalline alumina and hence the catalytic activity of silver–nanocrystalline alumina nanocomposite powders is better. On the basis of reported reduction mechanism [15,18], two processes occur during the reduction of 4-nitrophenol by $NaBH_4$ in the presence of silver–alumina nanocomposite powders (Fig. 5). The first one is the adsorption of 4-nitrophenolate and BH_4^- ions on the surface of the composite powder by chemisorption. The second process then starts in which the Ag nanoparticles help with the electron transfer from BH_4^- ions (donor) to the NO_2 group (acceptor) to form 4-aminophenolate ions. Desorption of 4-aminophenolate ions occurs afterwards from the surface of the catalyst. The catalytic activity of silver–alumina nanocomposite powders increases with the decrease of Ag concentration in the nanocomposite powders in the following order: Ag–nanocrystalline Al_2O_3 (S-6, [Ag acetate: alumina]=0.25:1) > Ag–nanocrystalline Al_2O_3 (S-4, 0.5:1) > Ag–nanocrystalline Al_2O_3 (S-1, 1:1).

The performance of the silver–nanocrystalline alumina nanocomposite powders as catalyst for the reduction of

Table 3
Reported studies on the reduction of 4-nitrophenol using different catalysts.

Sl. no.	Catalyst	Time of reduction (s)	Ref.
1.	Ag–Al_2O_3 nanocatalyst	1320	[14]
2.	Ag nanoparticles on SiO_2	300	[15]
3.	Polymer particles with dendrimer@SiO_2–Ag shell	<480	[16]
4.	Ag NP immobilized on polymer nanofibers	1800	[17]
5.	Silver nanoparticles	~1500	[19]
6.	CTAB-stabilized Au nanoparticles	6600	[30]
7.	Au nanoparticles–PMMA	600	[31]
8.	Ag–Al_2O_3 nanocomposite powders (S1–S6)	4–20	Present work

4-nitrophenol has been compared in Table 3 with those of the other reported nanostructured catalysts [14–17,19,30,31]. It can be noted that the performance of Ag–nanocrystalline alumina nanocomposite powders (e.g. sample S-6) is excellent compared to those of the other reported catalysts.

4. Conclusions

Silver–alumina nanocomposite powders have been successfully synthesized by a simple thermal decomposition approach. Two types of alumina (nanocrystalline and macro-crystalline) were employed for the synthesis of the nanocomposite powders which were characterized using a variety of analytical techniques. Nanocrystalline alumina acts as a better support compared to the macro-crystalline alumina and the silver nanoparticles are well dispersed on the surface of nanocrystalline alumina compared to macro-crystalline alumina. Catalytic activity of the silver–alumina nanocomposite powders as tested by the reduction of 4-nitrophenol indicates that the silver–nanocrystalline alumina nanocomposite powders act as better catalysts compared to silver–macro-crystalline alumina nanocomposite powders.

Acknowledgment

Ravi Kant Sharma would like to thank the Ministry of Human Resource and Development, Government of India, for providing financial support during the M.Tech. course of study. Thanks are also due to Institute Instrumentation centre, IIT Roorkee, for providing the facilities. The authors would like to thank Ms. Nisha Bayal for her help in revising the manuscript.

References

[1] D.K. Bozanic, S. Dimitrijevic-Brankovic, N. Bibic, A.S. Luyt, V. Djokovic, Silver nanoparticles encapsulated in glycogen biopolymer: morphology, optical and antimicrobial properties, Carbohydrate Polymers 83 (2011) 883–890.

[2] A. Nazari, S. Riahi, Improvement compressive strength of concrete in different curing media by Al_2O_3 nanoparticles, Materials Science and Engineering A 528 (2011) 1183–1191.

[3] M.I.F. Macedo, C.C. Osawa, C.A. Bertran, Sol–gel synthesis of transparent alumina gel and pure gamma alumina by urea hydrolysis of aluminum nitrate, Journal of Sol–Gel Science and Technology 30 (2004) 135–140.

[4] T. Bala, G. Armstrong, F. Laffir, R. Thornton, Titania–silver and alumina–silver composite nanoparticles: novel, versatile synthesis, reaction mechanism and potential antimicrobial application, Journal of Colloid and Interface Science 356 (2011) 395–403.

[5] C.L. Lu, J.G. Lv, L. Xu, X.F. Guo, W.H. Hou, Y. Hu, H. Huang, Crystalline nanotubes of γ -AlOOH and γ -Al_2O_3: hydrothermal synthesis, formation mechanism and catalytic performance, Nanotechnology 20 (2009) 215604/1–215606/9.

[6] M. Crisan, M. Zaharescu, V.D. Kumari, M. Subrahmanyam, D. Crisan, N. Dragan, M. Raileanu, M. Jitianu, A. Rusu, G. Sadanandam, Sol–gel based alumina powders with catalytic applications, Applied Surface Science 258 (2011) 448–455.

[7] A.K. Patra, A. Dutta, A. Bhaumik, Self-assembled mesoporous γ-Al_2O_3 spherical nanoparticles and their efficiency for the removal of arsenic from polluted water, Journal of Hazardous Materials 201–202 (2012) 170–177.

[8] L. Menon, W.T. Lu, A.L. Friedman, S.P. Bennett, D. Heiman, S. Sridhar, Negative index metamaterials based on metal–dielectric nanocomposites for imaging applications, Applied Physics Letters 93 (2008) 123117/1–123117/3.

[9] A.M. Jastrzebska, E. Radziun, M. Roslon, A.R. Kunicki, A.R. Olszyna, J. Dudkiewicz-Wilczynska, E. Anuszewska, E. Karwowska, In vitro assessment of antibacterial properties and cytotoxicity of Al_2O_3–Ag nanopowders, Advances in Applied Ceramics 110 (2011) 353–359.

[10] T. Sato, S. Goto, Q. Tang, S. Yin, $DeNO_x$ activity of Ag/γ-Al_2O_3 nanocomposites prepared via the solvothermal route, Journal of Materials Science 43 (2008) 2247–2253.

[11] H.J. Tang, F.Q. Wu, H.L. Wang, Y.H. Wei, Q.S. Li, Optical properties of Ag–Al_2O_3 nano-array composite structure, Optik 119 (2008) 134–138.

[12] Y.H. Yeom, M. Li, W.M.H. Sachtler, E. Weitz, A study of the mechanism for NO_x reduction with ethanol on γ-alumina supported silver, Journal of Catalysis 238 (2006) 100–110.

[13] K.I. Shimizu, A. Satsuma, T. Hattori, Catalytic performance of Ag–Al_2O_3 catalyst for the selective catalytic reduction of NO by higher hydrocarbons, Applied Catalysis B 25 (2000) 239–247.

[14] J.N. Solanki, Z.V.P. Murthy, Reduction of nitro aromatic compounds over Ag/Al_2O_3 nanocatalyst prepared in water-in-oil microemulsion: effects of water-to-surfactant mole ratio and type of reducing agent, Industrial and Engineering Chemistry Research 50 (2011) 7338–7344.

[15] S. Kundu, M. Mandal, S.K. Ghosh, T. Pal, Photochemical deposition of SERS active silver nanoparticles on silica gel and their application as catalysts for the reduction of aromatic nitro compounds, Journal of Colloid and Interface Science 272 (2004) 134–144.

[16] G. Dang, Y. Shi, Z. Fu, W. Yang, Polymer particles with dendrimer@SiO_2–Ag hierarchical shell and their application in catalytic column, Journal of Colloid and Interface Science 369 (2012) 170–178.
[17] S. Xiao, W. Xu, H. Ma, X. Fang, Size-tunable Ag nanoparticles immobilized in electrospun nanofibers: synthesis, characterization, and application for catalytic reduction of 4-nitrophenol, RSC Advances 2 (2012) 319–327.
[18] P. Liu, M. Zhao, Silver nanoparticle supported on halloysite nanotubes catalyzed reduction of 4-nitrophenol (4-NP), Applied Surface Science 255 (2009) 3989–3993.
[19] N. Pradhan, A. Pal, T. Pal, Silver nanoparticle catalyzed reduction of aromatic nitro compounds, Colloids and Surfaces A 196 (2002) 247–257.
[20] X. She, M. Flytzani-Stephanopoulos, The role of Ag–O–Al species in silver–alumina catalysts for the selective catalytic reduction of NO_x with methane, Journal of Catalysis 237 (2006) 79–93.
[21] E.G. Manoilov, Optical and photoluminescent properties of Ag/Al_2O_3 nanocomposite films obtained by pulsed laser deposition, Semiconductor Physics, Quantum Electronics and Optoelectronics 12 (2009) 298–301.
[22] M. Haji, T. Ebadzadeh, M.H. Amin, M. Kazemzad, T. Talebi, Gelcasting of Al_2O_3/Ag nanocomposite using water-soluble solid–salt precursor, Ceramics International 38 (2012) 867–870.
[23] S.H. Cheon, I.S. Han, S.H. Woo, Fabrication and characterization of alumina/silver nanocomposites, Journal of the Korean Ceramic Society 44 (2007) 343–348.
[24] S. Bhattacharyya, A. Gabashvili, N. Perkas, A. Gedanken, Sonochemical insertion of silver nanoparticles into two-dimensional mesoporous alumina, Journal of Physical Chemistry C 111 (2007) 11161–11167.
[25] G.L. Teoh, K.Y. Liew, W.A.K. Mahmood, Synthesis and characterization of sol–gel alumina nanofibers, Journal of Sol–Gel Science and Technology 44 (2007) 177–186.
[26] B.D. Cullity, S.R. Stock, Elements of X-ray Diffraction, Prentice Hall, 2001.
[27] M.S. Ghamsari, Z.A.S. Mahzar, S. Radiman, A.M. Abdul Hamid, S.R. Khalilabad, Facile route for preparation of highly crystalline γ-Al_2O_3 nanopowder, Materials Letters 72 (2012) 32–35.
[28] A.A. Anappara, S.K. Ghosh, P.R.S. Warrier, K.G.K. Warrier, W. Wunderlich, Impedance spectral studies of sol–gel alumina–silver nanocomposites, Acta Materialia 51 (2003) 3511–3519.
[29] S.D. George, A.A. Anappara, P.R.S. Warrier, K.G.K. Warrier, P. Radhakrishnan, V.P.N. Nampoori, C.P.G. Vallabhan, Photoacustic thermal characterization of Al_2O_3–Ag ceramic nanocomposites, Materials Chemistry and Physics 111 (2008) 38–41.
[30] K.Y. Lee, Y.W. Lee, J.H. Lee, S.W. Han, Effect of ligand structure on the catalytic activity of Au nanocrystals, Colloids and Surfaces A 372 (2010) 146–150.
[31] K. Kuroda, T. Ishida, M. Haruta, Reduction of 4-nitrophenol to 4-aminophenol over Au nanoparticles deposited on PMMA, Journal of Molecular Catalysis A 298 (2009) 7–11.